Electronic Supporting Information for:

Performance of Dye-Sensitized Quasi-Solid-State Solar Cell with Combined Anthocyanin-Ruthenium Photosensitizer

Eka Cahya Prima[a], Harbi Setyo Nugroho[b], Nugraha[b,c], Gema Refantero[b], Camelia Panatarani[d] and Brian Yuliarto[b,c]*

[a]*Department of Science Education, Faculty of Mathematics and Science Education, Universitas Pendidikan Indonesia, Bandung, Indonesia.*

[b]*Department of Engineering Physics, Faculty of Industrial Technology, Institut Teknologi Bandung, Bandung, Indonesia*

[c]*National Research Center of Nanotechnology (NRCN), Institut Teknologi Bandung, Bandung, Indonesia*

[d]*Department of Physics, Faculty of Mathematics and Natural Science, Universitas Padjadjaran, Bandung, Indonesia.*

** Corresponding Author's E-mail: brian@tf.itb.ac.id*

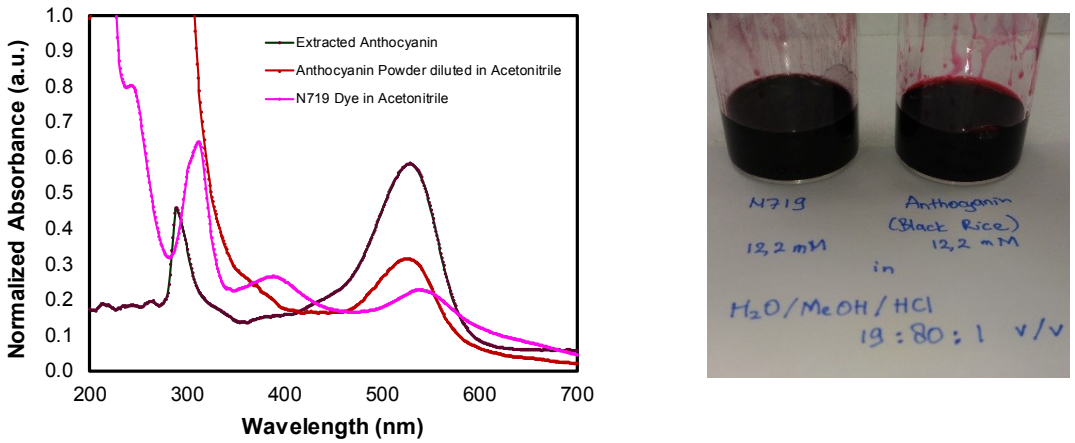

Figure S1. Dye absorbance comparison between Anthocyanin and N719 (left) and the dye extracts of anthocyanin and N719 (right)

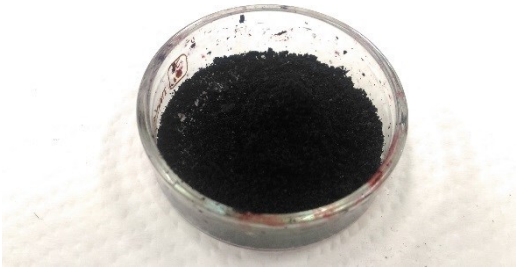

Figure S2. Anthocyanin powder

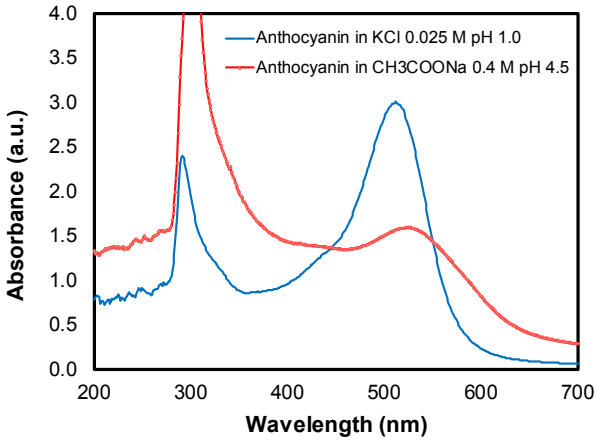

Figure S3. UV-Vis spectra for anthocyanin concentration analysis

The example of anthocyanin concentration calculation

$$A = (A_{512} - A_{700})_{pH1.0} - (A_{524} - A_{700})_{pH\ 4.5} \quad (1)$$
$$A = (3.0059 - 0.057934)_{pH1.0} - (1.58637 - 0.281571)_{pH\ 4.5}$$
$$A = 1.643167$$

$$Anthocyanin\ concentration\ = \frac{A\ \times 449.3\ \times DF\ \times 1000}{26900\ \times 1} mg/l$$
$$Anthocyanin\ concentration\ = \frac{1.643167\ \times 449.3\ \times 200\ \times 1000 mg}{26900\ \times 1 \qquad\qquad l}$$
$$Anthocyanin\ concentration\ = 5489.03 \frac{mg}{l}$$
$$Anthocyanin\ concentration\ = 12.2\ mM\ relative\ to\ the\ cyanidin-3-glucoside$$

Purification

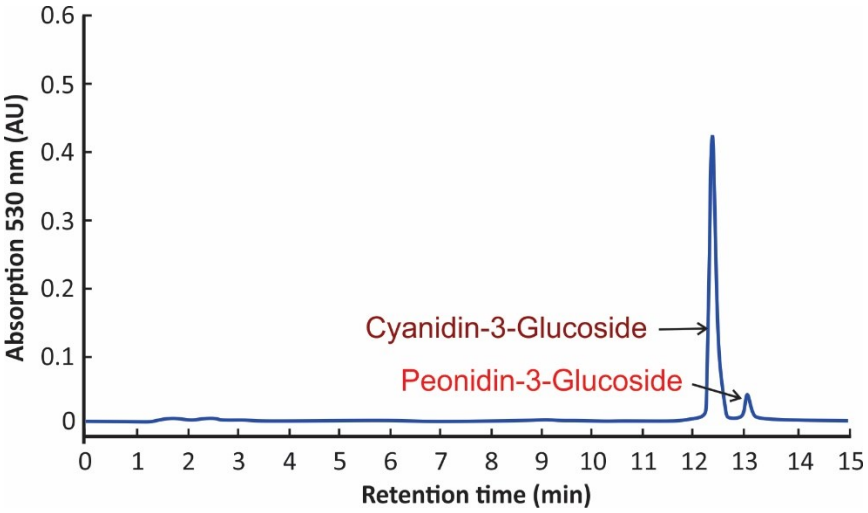

Figure S4. Identification of anthocyanin pigment in the black rice extract eluted with a linear gradient from 0.1 % TFA-H_2O to 0.1 % TFA-CH_3CN at 1 ml/min using HPLC

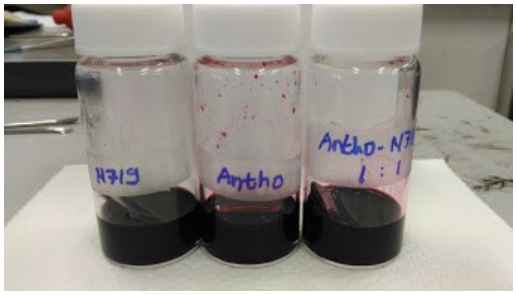

Figure S5. Pigment adsorption onto TiO_2 with the same concentration (12.2 mM after purification)

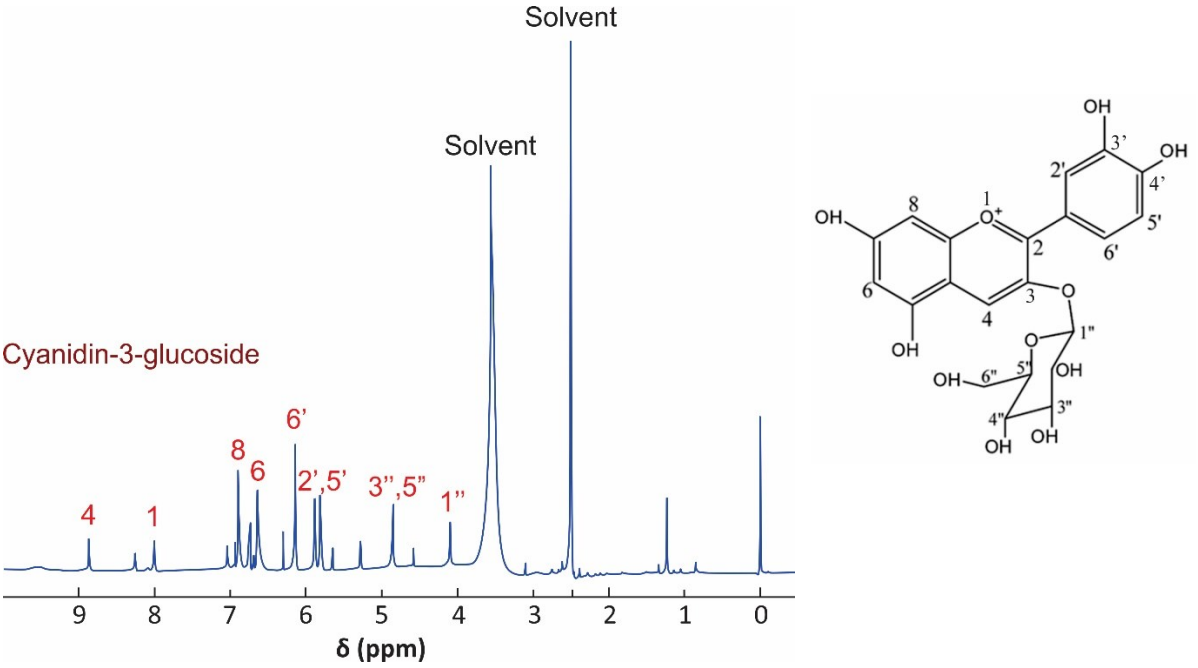

Figure S6. ^{1}H NMR analysis of cyanidin-3-glucoside

The anthocyanin chemical structure was analyzed using 1H NMR. The 0–4.80 ppm signals were attributed to protons in hexose units, except two intense high signals, assigned as the DMSO-d6. The intense peaks between 5.75 and 6.25 ppm might be attributed to hydroxyl protons in side chains of benzene rings. The signals at 6.25–7.25 ppm were due to protons from aromatic rings. The 8.04 ppm signal was assigned to protons at H-1 and the 8.94 ppm peak might be identified as H-4 as seen in the structure above.

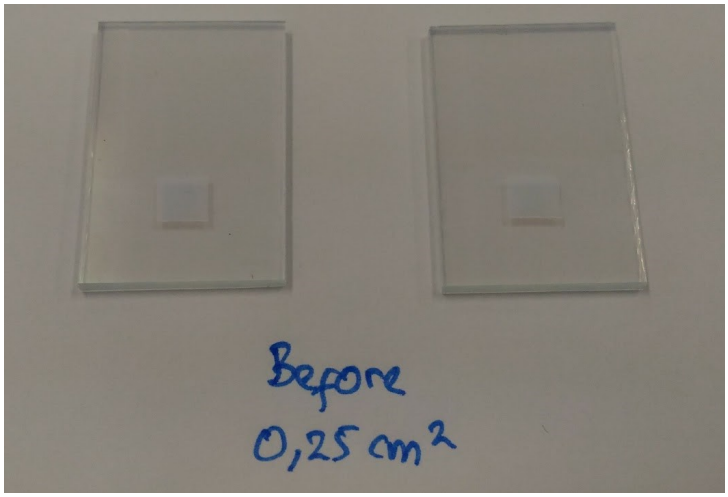

Figure S7. 0.25 cm^2 TiO_2 film before dye adsorption

Table S1

Vibration analysis of photosensitizer

Anthocyanin		**Anthocyanin-N719**		**N719**		**Reference**	**Analysis**
k (cm^{-1})	**T (%)**	**k (cm^{-1})**	**T (%)**	**k (cm^{-1})**	**T (%)**		
588.18	66.03	588.18	56.64	-	-	Anthocyanin	Stretching vibration of C-O-C aliphatic ether group from glucose
-	-	663.39	44.35	663.39	37.60	N719	Out-of-plane bending vibration of C-H and C-N
-	-	670-829	45.2-50.1	670-829	37.5-37.7	N719	Third order stretching vibration of C-H and C-N
1075.12	61.47	1075.12	41.63	-	-	Anthocyanin	In-of-plane bending vibration of C-H and stretching vibration of C-O
1639.20	60.26	1639.20	41.45	-	-	Anthocyanin	Stretching vibration of C=O aromatic group
-	-	1720.19	39.79	1720.19	27.20	N719	Stretching vibration of C=O and COOH group
-	-	2101.06	42.54	2101.06	26.45	N719	Stretching vibration of NCS group
2872-2975	47.2-58.1	2872-3600	36.1-47.5	2872-3600	23.2-27.9	N719; Anthocyanin	Stretching vibration of Alkanes Group C-H
2975-3600	47.2-58.1	2872-3600	36.1-47.5	2872-3600	23.2-27.9	N719; Anthocyanin	Stretching vibration of O-H

It can be seen that the 1H NMR and FT-IR analysis were consistent with the chemical structure of anthocyanins.

Table S2

Vibration analysis of photoelectrode

TiO_2		Analysis
k (cm-1)	**T (%)**	
460.7	4.3	Stretching vibration of -Ti-O
983.5	4.5	Stretching vibration of Ti-O-Ti
1000.9	4.5	Stretching vibration of Ti-O-Ti
1637.3	5.0	Stretching vibration of Ti-OH

Details of Dye-sensitized solar cell analysis[1]

- *HOMO-LUMO analysis*

Analysis The HOMO-LUMO levels are calculated using the following empirical Bredas [2]equations as given in Eq. (2) and (3)

$$E_{HOMO} = -e(E_{ox}^{onset} + 4.4) \quad (2)$$

$$E_{LUMO} = -e(E_{RED}^{onset} + 4.4) \quad (3)$$

- *Electrochemical impedance spectroscopy analysis*[3-14]

The photoanode properties of capacitance and conductivity are quantified using the electrochemical impedance spectroscopy method. By using this method, the diffusion length ($\boldsymbol{L_n}$), the charge lifetime ($\boldsymbol{\tau_n}$), and the charge extraction time ($\boldsymbol{\tau_d}$) are analyzed from the equivalent circuit. Figure 9(b) displays the equivalent circuit element model simplifying the system due to the low current restriction in which the impedance of electrolyte diffusion ($\boldsymbol{Z_d}$) is vanishingly small. The Nyquist plot, as seen in Fig. 9(a) explains the cell's impedance characteristic features using anthocyanin dye-sensitized solar cells. A large arc in a low-frequency semicircle is assigned to the dye recombination resistance ($\boldsymbol{R_r}$) coupled with $\boldsymbol{C_{\mu}}$, explaining the electrolyte-solid interface total capacitance. The small arc of the high-frequency semicircle indicates the charge transport resistance ($\boldsymbol{R_d}$) through the semiconductor of TiO_2 nanoparticles. At the bias potential of 0 V and the low-frequency condition, a large arc, which is resulted from the charge recombination and the back layer chemical capacitance, will lead to a higher

impedance. The work is controlled as a diffusion-recombination transmission line under the reflecting boundary conditions. Therefore, the electrons will be injected at the interface between the film TiO_2 semiconductor and the FTO. The electron will diffuse through the film or to the outer edge of the film where the electron transport is blocked.

In a restricted condition displaying at least two impedance spectra domains, as seen in Fig. 9, the domains of impedance are divided by the characteristic frequency (ω_d). The Warburg impedance happens in the high-frequency regime ($\omega \gg \omega_d$), which shows a short straight line in the impedance representation due to the diffusion. At the frequency which is lower than $\omega_{d'}$ the impedance behavior is commonly reflected or extracted at the end of the diffusion region. A large semicircle of lower frequency regime results in the longer electron lifetime and the faster electron transport through the TiO_2 film.

Equation (4) explains the transmission line impedance, excluding the effects of the series resistance ($\boldsymbol{R_S}$), the counter electrode resistance ($\boldsymbol{R_{pt}}$), and the counter electrode chemical capacitance ($\boldsymbol{C_{Pt}}$) as described in Fig. 9(b). For the impedance at low frequencies, the vertical feature intercept with the real axis results in 1/3 of the transport resistance ($\boldsymbol{R_t}$).

$$Z = \frac{1}{3}R_t + \frac{R_r}{1 + i\omega/\omega_r} \tag{4}$$

When electrons diffuse through a material, the true driving force for the chemical diffusion has two components including the first term of $\partial\mu/\partial n$ indicating a gradient in concentration and a gradient in chemical potential, and the second phenomenological coefficient of film thickness $\boldsymbol{L}$. The coefficient of chemical diffusion (D_n) is acquired from the EIS data, as expressed in Eq. (5).

$$D_n = \frac{L^2}{\tau_d} = \frac{L_n^2}{\tau_n} \tag{5}$$

Furthermore, the effective diffusion length ($\boldsymbol{L_n}$) is calculated using Eq. (6).

$$L_n = \sqrt{D_n \tau_n} = L\sqrt{\frac{\tau_n}{\tau_d}} = L\sqrt{\frac{R_r}{R_t}} \tag{6}$$

Figure 9 displays that L_n exceeds the thickness of the photoanode due to the $R_r >> R_t$. The τ_d corresponds to the transient time for the diffusion of an electron through the film injected at $x = 0$ through a distance L which is shown by Eq. (7)

$$\tau_d = R_t C_\mu = \frac{1}{\omega_d} = \frac{L^2}{D_n} \tag{7}$$

Rapid recombination commonly happens because the electrons react with tri-iodide ion I_3^- in the redox electrolyte before they recapture each other at the current collector. The phenomenon is explained by the electron lifetime, and it is represented by a large semicircle impedance, as expressed in Eq. (8). An excellent cell performance should show faster carrier extraction time (τ_d) and the slower recombination time (τ_n).

$$\tau_n = R_r C_\mu = \frac{1}{\omega_r} = \frac{L_n^2}{D_n} \tag{8}$$

Equation (9) describes the electron conductivity in the TiO_2 calculated from the resistance of electron transport.

$$\sigma_n = \frac{L}{A} R_t^{-1} \tag{9}$$

Where L is the film thickness, A is the photoanode projected area exposed through the Surlyn frame, and R_t is the macroscopic transport resistance.

References

1. E. C. Prima, N. N. Hidayat, B. Yuliarto, Suyatman and H. K. Dipojono, *Spectrochim. Acta Mol. Biomol. Spectrosc.* , 2017, **171**, 112-125.
2. J. L. Bredas, R. Silbey, D. S. Boudreaux and R. R. Chance, *J. Am. Chem. Soc.*, 1983, **105**, 6555-6559.
3. J. Bisquert and F. Fabregat-Santiago, in *Dye-sensitized Solar Cells*, ed. K. Kalyanasundaram, CRC Press, Switzerland, 2010, pp. 457-543.
4. A. B. F. Martinson, M. S. Góes, F. Fabregat-Santiago, J. Bisquert, M. J. Pellin and J. T. Hupp, *The Journal of Physical Chemistry A*, 2009, **113**, 4015-4021.
5. J. Bisquert, F. Fabregat-Santiago, I. Mora-Seró, G. Garcia-Belmonte and S. Giménez, *J. Phys. Chem. C* 2009, **113**, 17278-17290.
6. J. Bisquert, F. Fabregat-Santiago, I. Mora-Seró, G. Garcia-Belmonte and S. Giménez, *The Journal of Physical Chemistry C*, 2009, **113**, 17278-17290.
7. G. Garcia-Belmonte, A. Munar, E. M. Barea, J. Bisquert, I. Ugarte and R. Pacios, *Organic Electronics*, 2008, **9**, 847-851.
8. J. Bisquert, *J. Phys. Chem. B* 2004, **108**, 2323-2332.
9. J. Bisquert, G. Garcia-Belmonte and Á. Pitarch, *ChemPhysChem*, 2003, **4**, 287-292.
10. J. Bisquert, *Physical Chemistry Chemical Physics*, 2003, **5**, 5360-5364.

11. J. Bisquert and V. S. Vikhrenko, *Electrochim. Acta*, 2002, **47**, 3977-3988.
12. J. Bisquert, *J. Phys. Chem. B*, 2002, **106**, 325-333.
13. J. Bisquert, *The Journal of Physical Chemistry B*, 2002, **106**, 325-333.
14. J. Bisquert and A. Compte, *J. Electroanal. Chem.* , 2001, **499**, 112-120.